Radiative cooling force in atoms with multiplet structure

Arturo Bambini
Istituto di Elettronica Quantistica, Consiglio Nazionale delle Ricerche, via Panciatichi 56/30, I-50127 Firenze, Italy

Alessandro Agresti
Dipartimento di Fisica della Università di Firenze, Sezione di Fisica Superiore, via Santa Marta 3, I-50139 Firenze, Italy
(Received 24 February 1997)

This paper extends the calculation of laser cooling forces on atoms with magnetic degeneracy to the case where the excited state is composed by a multiplet of levels with arbitrary energy separation. The sub-Doppler force that arises in the σ_+,σ_- field configuration is found to be strongly affected if other atomic levels lie close to the excited level of the cooling transition. The paper examines in detail the case in which the excited multiplet comes from spin-orbit coupling of angular momentum $L=1$ and spin $S=1$, forming the $J_e=0$, $J_e=1$, and $J_e=2$ energy levels. The cooling transition $J_g=1\leftrightarrow J_e=2$ shows the sub-Doppler structure due to magnetic degeneracy. The force is modified by the two other transitions (if sufficiently close), even if these do not provide any mechanical effect on the atom when acting alone. The paper presents a detailed scheme for the construction of the relevant optical Bloch equations for the present case, which can be generalized to treat more complex atomic structures. The solutions to these equations are then discussed; several cases of energy separation are worked out and the ensuing graphs of the radiative force are shown. The calculations were carried out in both low- and strong-field regimes. [S1050-2947(97)10309-2]

PACS number(s): 32.80.Pj

I. INTRODUCTION

Laser cooling below the ''Doppler'' limit temperature $T_D=\hbar\gamma/(2k_B)$ [1] was observed in several experiments by the end of the 1980s [2,3]. It was soon realized that the two-level system, used to describe the atomic transitions induced by the laser beams and derive the radiative force acting onto the atom, was completely inadequate [4,5], as it predicted limit temperatures several times higher than the ones actually measured in optical molasses. The magnetic degeneracy of the levels involved in the transition was soon recognized to be the ultimate cause of such behavior [6,7].

Magnetic sublevels enter the process in radically different ways, depending on the polarization of the laser beams used to cool down the atomic gas. Two typical schemes of laser cooling were analyzed in detail [6]. In the first one two counterpropagating beams, with linear polarization and polarization axes mutually orthogonal, are used to damp the motion of the atom. The laser frequency is tuned close to an atomic transition between a $J_g=1/2$ ground level and a $J_e=3/2$ excited level. Under such excitation, a dipole force is exerted on the atoms moving with low velocities along the axis of the fields' propagation: when the laser frequency is tuned below the atomic resonance, the force acts against the atomic motion, providing an effective frictional force. In the second scheme, two counterpropagating laser beams with opposite circular polarization are used instead. In this case, the lowest magnetic degeneracy that allows for a sub-Doppler cooling is one with $J_g=1$ in the ground state, and $J_e=2$ in the excited state. Under such conditions, a radiative force arises that is mostly due to the unbalanced radiation pressure exerted by the two beams. Tuning again the laser frequency below the atomic resonance, the resulting radiation force acts as a viscous force proportional to the atomic velocity v, when v is sufficiently low, providing an effective sub-Doppler cooling of the atomic species. Both these schemes were investigated for isolated transitions, i.e., when the levels involved in the cooling mechanism are well separated from all other atomic levels. A detailed description of the processes involved in these cooling schemes can be found in Ref. [8].

In this paper we discuss several aspects of sub-Doppler laser cooling of atoms with Zeeman sublevels by means of two coaxial and counterpropagating laser beams with the same frequency ω_L and the same amplitude: a σ_+ circularly polarized field propagating in the positive direction of the z axis, and a σ_- circularly polarized field propagating in the negative direction of the z axis. In Refs. [6,8] it was shown that, with such a configuration, the polarization of the resulting field is always linear, but the polarization axis changes its direction along z: indeed, the polarization axis of the resulting field rotates in the xy plane as z varies, completing a full rotation of 360° when z has changed by an optical wavelength λ.

An atom moving along the z axis will therefore see a linearly polarized field with a polarization axis rotating in the x-y plane. Let the Zeeman sublevels of the atom refer to the quantization axis directed along z, and choose the orientation of the other two axes x and y in such a way that the field is always polarized along the y axis. In order to satisfy this condition, we must choose a rotating reference frame. The state amplitudes of the Zeeman sublevels in such a rotating frame are obtained from the state amplitudes in the fixed frame by applying the transformation $\exp(-i\phi J_z)$, where J_z is the z component of the angular momentum operator. Therefore, they vary according to

$$\psi_m^{\text{rotating}}=\psi_m^{\text{fixed}}e^{-im\phi}, \tag{1.1}$$

where ϕ is the angle of rotation and m the magnetic quantum

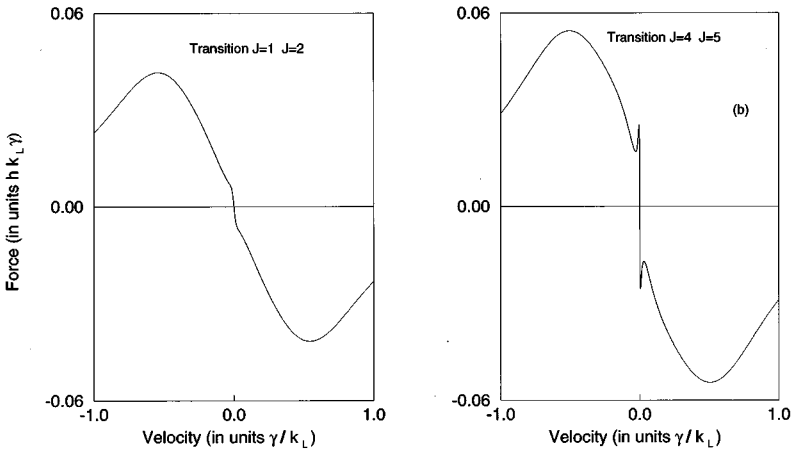

FIG. 1. Gradient polarization forces at low field intensities in the σ_+, σ_- configuration. (a) transition $J_g=1\leftrightarrow J_e=2$. (b) transition $J_g=4\leftrightarrow J_e=5$. The field amplitude corresponds to a reduced Rabi frequency of 0.2795γ (see Sec. VI).

number of the Zeeman sublevel. If the atom moves with a velocity v along the z axis, and we choose the rate of rotation of the reference frame so that the atom, in such a frame, sees a linearly polarized field *always* directed along the y axis, then $\phi=k_L v t$, where k_L is the magnitude of the laser fields' wave vector. Thus, the rotation of the reference frame manifests itself as a shift ΔE_m in the energy of the sublevels,

$$\Delta E_m = m\hbar k_L v, \tag{1.2}$$

which can be traced back to a fictitious magnetic field **B** directed along the z axis (Larmor's theorem). The frequency of the precession induced by this field is $k_L v$. Note that the field **B** is constant in both magnitude and direction as long as the atom maintains its velocity v constant along the z axis.

The fictitious magnetic field **B** is the source of a motion induced orientation of the atomic ground state: in particular, it was shown that, if the atomic velocity v along the z axis is positive, and the common frequency of the two laser beams is slightly detuned to the red of the atomic transition, the population of the $m=-1$ sublevel in the stationary regime is larger than the population of the $m=+1$ sublevel. Thus, the probability for such an atom to absorb a photon from the σ_- component of the field is larger than the probability of absorbing a photon from the σ_+ component. This in turn yields an unbalanced radiation pressure exerted by the two fields, with a net, velocity dependent, viscous force, larger than the one predicted by the cooling theories based on a simple two level model. This force has been shown in Refs. [6,8] to be mostly of a dissipative character. A further correction to the cooling force is provided by the coherence that arises between the $m=-1$ and $m=+1$ sublevels of the ground state (the reactive component of the force), but this does not change the conclusions outlined above. The new force arising from polarization gradients is effective in a range of atomic velocities for which $k_L|v|\ll\gamma'$, where γ' is the rate of optical pumping among the ground state's sublevels induced by the circularly polarized fields. Optical pumping occurs through several absorption processes followed by spontaneous emission processes: if the field amplitude is low enough, as in several experimental apparatuses used in laser cooled molasses, the optical pumping rate γ' is much smaller than the rate of spontaneous emission processes γ. In the opposite limit, i.e., when $k_L|v|$ is much larger than γ' and gets closer to the damping rate γ of the atomic transition, the new mechanism that results in a stronger force disappears, and the usual Doppler force of the two level atom is restored.

The calculation of the force for the $J_g=1\leftrightarrow J_e=2$ transition leads to the graph shown in Fig. 1(a). One can see here that, at low velocities, the force has a steep variation with v, while at larger values of v the force gets a smoother behavior, since the effects brought in by the magnetic degeneracy of the atomic states involved in the transition have disappeared, as mentioned above.

A similar calculation carried out for a $J_g=4\leftrightarrow J_e=5$ transition, such as the one involved in the laser cooling of cesium atoms, is shown in Fig. 1(b) (details of these calculations will be given below). One can see that the force arising from polarization gradient effects in the proximity of $v\approx 0$ is sloping even more sharply. This is not surprising, since the magnetic alignment induced by the fictitious field **B** is remarkably larger in states with high magnetic degeneracy. It should be noted that the friction force arising near $v=0$ may even exceed the Doppler force in transitions involving levels with high magnetic degeneracy. In the graph of Fig. 1(b) this results in a peak of the force at $v\sim\pm 0.01\gamma/k_L$, where the highest magnetic polarization of the atoms is achieved. At larger atomic velocities such an effect is washed out and the only remaining force is the Doppler force.

However, the effects due to a larger friction force in a transition with higher magnetic degeneracy are somewhat reduced by an enhanced diffusion coefficient [9], whose value ultimately sets the limit temperature that can be reached for the atomic species under consideration.

As noted above, the minimal magnetic degeneracy in the ground state required to observe motion-induced orientations and the new friction force is the one associated with a total angular momentum $J=1$. It is obvious that these effects cannot be present if the ground state is not degenerate. Yet, magnetic degeneracy is, in most cases, brought in by spin-orbit coupling and/or hyperfine interactions. For instance, in the case of cesium D_2 transition, the ground state $6s\ ^2S_{1/2}$ has the orbital angular momentum $L=0$, and the excited state $6p\ ^2P_{3/2}$ has $L=1$. These states couple with the electronic spin $S=1/2$ to form $J=1/2$ and $J=3/2$ angular momentum states. Finally, the nuclear spin $I=7/2$ brings the hyperfine structure $F=3$ and $F=4$ in the ground state and $F=2$, $F=3$, $F=4$, $F=5$ in the excited state. Magnetic de-

generacy is then associated with the presence of other levels of the multiplet, which in turn may affect the magnetic alignment and the ensuing force. Moreover, the strongest coupling of the electromagnetic field with the atom occurs through the electric dipole interaction, which involves only transitions among states with different *orbital* angular momentum. It is therefore of interest to investigate how the new kind of force, in a transition $L=0 \leftrightarrow L=1$, emerges because of the spin-orbit coupling that brings magnetic degeneracy of the two states involved in the transition.

In this paper we consider an atom with an $L=0$ ground state and an $L=1$ excited state. The orbital angular momentum is then coupled with a fictitious spin $S=1$ (which forms a $J=1$ ground state and a multiplet $J=0$, $J=1$, and $J=2$ in the excited state) and we study the emergence of the polarization gradient force in a σ_+, σ_- configuration, as the coupling grows from zero (where the only force present is the Doppler force since there is no magnetic degeneracy in the ground state with $L=0$) to a finite value. When the frequency separation in the multiplet is much larger than every other frequency that enters the problem, we expect to recover, at low atomic velocities, the polarization gradient force shown in Fig. 1. On the other hand, when the frequency separation is not so large, we expect to find deviations from the ideal behavior, and ultimately the disappearance of the sub-Doppler force when the spin-orbit coupling is vanishingly small. This is not of a mere academic interest: in real cases, such as when the atomic species in the optical molasses is an alkaline atom, the frequency separation among excited sublevels are often of the order of a few times the spontaneous decay rate γ. In such cases, we expect to find substantial deviations from the cooling force arising from a $J_g \leftrightarrow J_e$ (with $J_e=J_g+1$) transition. In this paper, we limit ourselves to an evaluation of the cooling force under these circumstances, without considering effects of the spin-orbit coupling on the diffusion coefficient.

This paper is organized as follows. In Sec. II, we review the basic concepts of the radiation pressure force exerted by two counterpropagating waves onto a linear oscillator and an atomic system with magnetic degeneracy. In Sec. III, we describe the atomic internal structure in our model: the ground state, with orbital angular momentum $L=0$, and the excited state, with angular momentum $L=1$. Spin-orbit coupling ($S=1$) is then added and gives rise to a multiplet structure in the excited state, with $J=0$, 1, and 2 levels having different energies, while the ground state gets a total angular momentum $J=1$. In Sec. IV, we derive the optical Bloch equations in the (L,S,M_L,M_S) and the (L,S,J,M_J) bases. Strong spin-orbit coupling is considered in the next section: we show there that optical transitions from the ground state ($J=1$) to either a $J=0$ or a $J=1$ excited state do not add to the force exerted onto the atom. Not only do these transitions not provide any sub-Doppler contributions to the force [8], they are also not capable of producing any effective mechanical effect on the atom. In Sec. VI we discuss the case of weak spin–orbit coupling, where the multiplet splitting is small and interference effects arise among transitions to the excited levels. In such cases, it may be expedient to tune the laser field below the lowest resonance, but then the cooling force is affected by the interference effects and the ensuing force turns out to be quite different from the ideal case of isolated transitions. Finally, Sec. VII summarizes the main results derived in this paper.

II. THE COOLING FORCE

A. The optical block equations

The friction force exerted on the atoms by counterpropagating laser beams has been the subject of extensive investigations (see, for instance, Ref. [10] and references therein). It arises because the internal state of a moving atom does not adjust itself immediately to the variations of the laser field experienced during its motion. The cooling force could also be derived in a simple way by considering a linear and damped oscillator, coupled to two driving fields having slightly different frequencies, such as those resulting from the Doppler effect in a reference frame that moves with the atom. Carrying out the calculations, one would find that the oscillator experiences a force given by

$$\mathcal{F}=\frac{\gamma g_0^2}{2\omega_0\{\gamma^2+4(\omega_0-\omega')^2\}}-\frac{\gamma f_0^2}{2\omega_0\{\gamma^2+4(\omega_0-\omega)^2\}}, \tag{2.1}$$

where f_0 and g_0 are the amplitudes of the driving fields, ω,ω' are their frequencies, γ is the damping constant, and ω_0 is the oscillator frequency. Equation (2.1) is quite general in all respects, except that it lacks saturation. It contains only the dissipative component, since the amplitude of the driving fields is assumed to be constant.

A widely used model to evaluate the force exerted by the electromagnetic field on an atom is one in which the generalized optical Block equations are introduced to describe the response of the atom to the field. Saturation effects are automatically taken into consideration when using the Block equations to evaluate the atomic polarizability. Magnetic degeneracy of the levels is included in the description, since it plays a relevant role in the process.

For the sake of completeness, we describe here the basic steps in deriving the optical Bloch equations (OBE) in a system with magnetic degeneracy. This will prove useful later in this paper, when the OBE will be generalized to include the effects of spin-orbit coupling. We consider the unidimensional problem only, in which both the atomic motion and the propagation of the electromagnetic field occur in the same direction, along which we take the z axis. This axis is also taken as the quantization axis for the eigenstates of angular momentum. We disregard for the moment the multiplet structure of the excited state, and consider only transitions between the ground state with total angular momentum J_g and the excited state with total angular momentum J_e. The external degrees of freedom on the atom, i.e., its motion along the z axis, are considered only in a classical way, which is a valid approximation as long as the atomic speed is sufficiently large. The internal degrees of freedom are fully described by the density operator whose equations of motion are given by

$$i\frac{d\sigma}{dt}=[H,\sigma]+i\left(\frac{d\sigma}{dt}\right)_{\text{damp}},$$

where $[H,\sigma]$ is the commutator of the density operator with the Hamiltonian of the system, and $(d\sigma/dt)_{\rm damp}$ is a term that accounts for the damping in the system due to the spontaneous emission processes.

The field is made up of two counterpropagating running waves, of circular polarizations σ_+ and σ_-:

$$\mathbf{E}(z,t)=\mathbf{E}(\sigma_+,z,t)+\mathbf{E}(\sigma_-,z,t), \tag{2.2}$$

where

$$\mathbf{E}(\sigma_+,z,t)=-\frac{\mathcal{E}}{\sqrt{2}}(\hat{\boldsymbol{i}}+i\hat{\boldsymbol{j}})e^{-i(\omega_L t-k_L z)}+\text{c.c.} \tag{2.3a}$$

and

$$\mathbf{E}(\sigma_-,z,t)=\frac{\mathcal{E}'}{\sqrt{2}}(\hat{\boldsymbol{i}}-i\hat{\boldsymbol{j}})e^{-i(\omega_L t+k_L z)}+\text{c.c.} \tag{2.3b}$$

The two components of the field have the same frequency ω_L and the wave vector $|\mathbf{k}_L|=k_L$ pointing in opposite directions. The atom-field coupling occurs via the electric dipole coupling,

$$-\mathbf{d}\cdot\mathbf{E}(z,t)=-\{\mathcal{E}T_{+1}e^{-i(\omega_L t-k_L z)}+\mathcal{E}'T_{-1}e^{-i(\omega_L t+k_L z)}\}+\text{H.c.}, \tag{2.4}$$

where we have used the tensorial components of the electric dipole operator

$$T_{+1}=-\frac{1}{\sqrt{2}}(x+iy),\quad T_{-1}=\frac{1}{\sqrt{2}}(x-iy). \tag{2.5}$$

Atomic units are used in which the Planck's constant $\hbar$ and the charge of the electron e are set equal to unity. Introducing the symbols

$$F=\mathcal{E}e^{-i(\omega_L t-k_L z)},\quad G=\mathcal{E}'e^{-i(\omega_L t+k_L z)} \tag{2.6}$$

the complete coupling operator can be written in the form

$$-\mathbf{d}\cdot\mathbf{E}(z,t)=-\{FT_{+1}+F^*(T_{+1})^\dagger+GT_{-1}+G^*(T_{-1})^\dagger\}. \tag{2.7}$$

In what follows, we will denote by σ the atomic density operator. Latin letters m,n will be used as indices of the ground state sublevels, and greek letters α,β as indices of the excited state sublevels. The time evolution of the atomic density operator driven by the field of circular polarization σ_+ alone is described by the equation of motion

$$i\frac{d\sigma_{mn}}{dt}=F^*\mathfrak{RC}(\beta,-1,m)\langle\beta|\sigma|n\rangle-F\mathfrak{RC}(n,+1,\alpha)\langle m|\sigma|\alpha\rangle, \tag{2.8a}$$

$$i\frac{d\sigma_{\alpha m}}{dt}=F\mathfrak{RC}(n,+1,\alpha)\langle n|\sigma|m\rangle-F\mathfrak{RC}(m,+1,\beta)\langle\alpha|\sigma|\beta\rangle, \tag{2.8b}$$

$$i\frac{d\sigma_{\alpha\beta}}{dt}=F\mathfrak{RC}(m,+1,\alpha)\langle m|\sigma|\beta\rangle-F^*\mathfrak{RC}(\beta,-1,n)\langle\alpha|\sigma|n\rangle \tag{2.8c}$$

and similarly for the terms arising from the coupling with the σ_- component,

$$i\frac{d\sigma_{mn}}{dt}=G^*\mathfrak{RC}(\beta,+1,m)\langle\beta|\sigma|n\rangle-G\mathfrak{RC}(n,-1,\alpha)\langle m|\sigma|\alpha\rangle, \tag{2.9a}$$

$$i\frac{d\sigma_{\alpha m}}{dt}=G\mathfrak{RC}(n,-1,\alpha)\langle n|\sigma|m\rangle-G\mathfrak{RC}(m,-1,\beta)\langle\alpha|\sigma|\beta\rangle, \tag{2.9b}$$

$$i\frac{d\sigma_{\alpha\beta}}{dt}=G\mathfrak{RC}(m,-1,\alpha)\langle m|\sigma|\beta\rangle-G^*\mathfrak{RC}(\beta,+1,n)\langle\alpha|\sigma|n\rangle. \tag{2.9c}$$

where we have introduced the symbols $\mathcal{C}(m,q,\alpha)$ and $\mathcal{C}(\alpha,q,m)$ defined by

$$\mathcal{C}(m,q,\alpha)=\frac{\langle J_g,K,m,q|J_g,K,J_e,\alpha\rangle}{\sqrt{2J_e+1}}, \tag{2.10a}$$

$$\mathcal{C}(\alpha,q,m)=\frac{\langle J_e,K,\alpha,q|J_e,K,J_g,m\rangle}{\sqrt{2J_g+1}}. \tag{2.10b}$$

$\langle J_g,K,m,q|J_g,K,J_e,\alpha\rangle$ and $\langle J_e,K,\alpha,q|J_e,K,J_g,m\rangle$ denote Clebsch-Gordan coefficients, $\mathfrak{R}$ is the reduced matrix element of the transition,

$$\mathfrak{R}=(g\|T\|e), \tag{2.11}$$

and K is the rank of the coupling spherical tensor, in our case the electric dipole vector, for which $K=1$. Using the symmetry properties of the Clebsch-Gordan coefficients, one can show that $\mathcal{C}(\alpha,q,m)=\mathcal{C}(m,-q,\alpha)$. Exchanging the states m and α in this relation would change the sign of the coefficient for $q=0$, but, for our case of circularly polarized fields, the only components that are allowed are those with $q=\pm1$, since the quantization axis coincides with the axis along which the electromagnetic waves propagate. In deriving the equations for the density matrix elements, we have discarded terms oscillating at $2\omega_L$ (rotating wave approximation). According to this approximation, the off-diagonal elements of the density matrix are redefined as

$$\tilde{\sigma}_{\alpha m}=\sigma_{\alpha m}e^{i\omega_L t}. \tag{2.12}$$

accordingly, the time dependence in F and G will disappear, and the field amplitudes are replaced by

$$\tilde{F}=\mathcal{E}e^{ik_L z},\quad \tilde{G}=\mathcal{E}'e^{-ik_L z}. \tag{2.13}$$

The tilde will be omitted in what follows.

To these equations we have to add the terms of the free evolution of the system and the damping terms due to spontaneous emission. While the inclusion of the free evolution

terms is straightforward, keeping account of the spontaneous emission processes requires some algebraic effort.

Decay from the upper levels into the lower ones can occur through spontaneous emissions of photons with any polarizations. The basic assumption is made that the spontaneous emission processes are statistically independent processes. Thus, with a straightforward generalization of the equation governing the radiative decay for a two level system, we write the equation that describes the decay processes for a multilevel atom as [11–13]

$$\left(\frac{d\sigma}{dt}\right)_{\text{damp}} = \sum_q \left\{ -\frac{1}{2}(S_\uparrow^{(q)} S_\downarrow^{(q)} \sigma + \sigma S_\uparrow^{(q)} S_\downarrow^{(q)}) + S_\downarrow^{(q)} \sigma S_\uparrow^{(q)} \right\}, \tag{2.14}$$

where $S_\uparrow^{(q)}$ ($S_\downarrow^{(q)}$) is the raising (lowering) operator for electric dipole transitions induced by the q component of the tensor $T^{(1)}$. Note that the raising and lowering operators have been defined so as to include the damping constant. In this way, the Bloch equations for an atom with magnetic sublevels are readily written.

B. Evaluation of the cooling force

To evaluate the radiative force acting on the atom, we must find the atomic polarization induced by the field in the stationary state. We therefore have to integrate the full system of equations, starting from arbitrary initial conditions, until a situation is reached in which the populations do not vary when time elapses. It is expedient to refer the atomic system to a rotating system of coordinate axes that moves with the atom. The z axis is taken along the direction of field propagation. The x and y axes are made to rotate about the z axis, in such a way that, in this reference frame, the atom sees always a linearly polarized field. As mentioned above, the effect of the rotating reference frame is taken into account by a fictitious magnetic field **B**, directed along the rotating axis (i.e., the z axis). Since the latter field is constant as long as the atom keeps moving with the same velocity, the interaction between the atom and the field is described by a time independent term. Thus, we expect that in such a moving rotating frame of reference, each element of the density matrix reaches a stationary value, independent of time.

The indices of the matrix elements σ_{kl} run over the entire set of the states considered here, $2J_g+1$ for the ground state's sublevels, and $2J_e+1$ for the excited state's sublevels. Within each manifold, states are numbered in the order of ascending magnetic number. The transformation of the density matrix from the fixed reference frame to the moving rotating frame is performed by

$$\sigma^{(\text{rot})} = \tau^\dagger \{\sigma^{(fix)}\} \tau, \tag{2.15}$$

where τ is a diagonal matrix given by

$$\tau = \begin{pmatrix} e^{-iJ_g\phi} & & & & & \\ & \cdots & & & & \\ & & e^{+iJ_g\phi} & & & \\ & & & e^{-iJ_e\phi} & & \\ & & & & \cdots & \\ & & & & & e^{+iJ_e\phi} \end{pmatrix} \tag{2.16}$$

and ϕ is equal to $k_L v t$.

Another method to solve the equations and find the stationary values of the matrix elements $\sigma_{ik}^{(\text{rot})}$ is to solve the linear system of equations

$$\frac{d\sigma_{ik}^{(\text{rot})}}{dt} = 0 \tag{2.17}$$

in the unknowns $\sigma_{ik}^{(\text{rot})}$ that represent the stationary (i.e., time independent) values of the density matrix elements. The derivative of each matrix element $\sigma_{ik}^{(\text{rot})}$ can be expressed as a linear combination of the matrix elements themselves. The system (2.17) is homogeneous but its determinant is null; the matrix elements are then completely determined by imposing another condition on them, namely, that the total population $\Sigma_i \sigma_{ii}$ of both the ground and the excited states be 1. The evaluation of the eigenvalues of the time evolution matrix for the matrix elements $\sigma_{ik}^{(\text{rot})}$ gives also useful insights into the problems connected to numerically integrating the full system of differential equations, such as the time required to reach the stationary regime, which is determined by the slowest time scale in the system, i.e., the optical pumping characteristic time $1/\gamma'$, and, possibly, the very existence of such a regime. It is expedient to write the time evolution matrix as a real matrix, splitting the matrix elements $\sigma_{ik}^{(\text{rot})}$ and $\sigma_{ki}^{(\text{rot})}$ into their real and imaginary parts.

Having found the stationary values of the density operator matrix elements, in one way or the other, we can determine the atomic polarization and hence the radiative force. We define the symbols

$$\mathcal{P}_+ = \frac{\Re}{\sqrt{2}} \sum_{\alpha,m} \langle m|\sigma|\alpha\rangle \mathcal{C}(m,+1,\alpha), \tag{2.18a}$$

$$\mathcal{P}_- = \frac{\Re}{\sqrt{2}} \sum_{m,\alpha} \langle m|\sigma|\alpha\rangle \mathcal{C}(m,-1,\alpha) \tag{2.18b}$$

to indicate the atomic polarization induced by the σ_+ and σ_- components of the field. In Eqs. (2.18a) and (2.18b), the matrix elements $\langle m|\sigma|\alpha\rangle$ give the steady state coherences in the fixed reference frame. According to Eq. (2.15), these are given, in terms of the stationary values for $\sigma_{ik}^{(\text{rot})}$, by the relations

$$\mathcal{P}_+ = \mathcal{P}_+^{(\text{rot})} e^{-ik_L v t}, \tag{2.19a}$$

$$\mathcal{P}_- = \mathcal{P}_-^{(\text{rot})} e^{+ik_L v t}. \tag{2.19b}$$

We find then the expression for the radiative force exerted on the atom by the combined action of the two field components

$$\mathcal{F} = 2\sqrt{2} k_L [F\ \text{Im}(\mathcal{P}_+^{(\text{rot})}) - G\ \text{Im}(\mathcal{P}_-^{(\text{rot})})]. \tag{2.20}$$

Both graphs in Fig. 1 were obtained by evaluating Eq. (2.20) for the transitions $J_g = 1 \leftrightarrow J_e = 2$ [see Fig. 1(a)] and $J_g = 4 \leftrightarrow J_e = 5$ [see Fig. 1(b)].

It is to be noted that Eq. (2.20) expresses the total radiative force acting on the atom because of its interaction with the electromagnetic field. The force has reactive and dissipative components (see Ref. [8] for a complete discussion of

this subject) that arise from different physical mechanisms, but we prefer to use Eq. (2.20), which gives the total force, i.e., the sum of the two components, since the latter are difficult to disentangle in a strong field regime. Moreover, Eq. (2.20) is more apt for numerical calculations.

III. SPIN-ORBIT INTERACTION

We consider here a simplified atomic model to describe how spin-orbit coupling affects the cooling force exerted by the electromagnetic field. The atom is basically a two level system, in which the lower (ground) state has orbital angular momentum $L=0$, and the excited level has orbital angular momentum $L=1$. In such a system, the force exerted by the two counterpropagating, circularly polarized fields, in the same unidimensional geometry described in Sec. II, would be the Doppler force alone. However, we add a fictitious spin $S=1$ to the system, and the spin-orbit coupling gives rise to a multiplet of excited levels with $J_e=0$, $J_e=1$, and $J_e=2$, having different energies. The ground state gets a total angular momentum $J_g=1$. The force exerted by the laser fields tuned near the resonance $J_g=1 \leftrightarrow J_e=2$ includes the new kind of force, and allows for sub-Doppler cooling. Thus, the rise of the new force is entirely due to the spin-orbit coupling. This can be seen in another way yet: if the ground state is an $L=0$ state, with any spin component, and we disregard couplings with the electromagnetic field other than the electric dipole coupling, then transitions are induced by the field only towards the sublevels $M_L=+1$ and $M_L=-1$ of the excited state. In the absence of a spin-orbit interaction, which couples these sublevels with others having *different* spin component, any sublevel of the excited state would decay to a ground state $L=0$ sublevel having the same spin component, thus preventing the formation of a motion-induced orientation in the ground state and coherences among its sublevels. Thus the only available cooling force would be the Doppler force. We will see later in this paper that the strength of the spin-orbit coupling greatly affects the formation of the motion-induced orientation of the ground state and the coherences among the ground sublevels.

It should be noted that a situation in which transitions occur among $L=0$ and $L=1$ states is typical of many atomic species used in generating laser-cooled atomic molasses, although the spin may be much larger than the one ($S=1$) considered here.

The whole atomic system in our model contains twelve sublevels, three in the ground state, and nine in the excited states. We label these sublevels, in the two bases $\{L,M_L\}$ and $\{J,M_J\}$ (see Table I).

TABLE I. States of the atomic system in the (L,M_L), (J,M_J) bases.

	L,M_L basis		J,M_J basis	
State 1:	$M_S=-1$	$M_L=0$	$J_g=1$	$M_J=-1$
State 2:	$M_S=0$	$M_L=0$	$J_g=1$	$M_J=0$
State 3:	$M_S=1$	$M_L=0$	$J_g=1$	$M_J=1$
State 4:	$M_S=-1$	$M_L=-1$	$J_e=2$	$M_J=-2$
State 5:	$M_S=-1$	$M_L=0$	$J_e=1$	$M_J=-1$
State 6:	$M_S=0$	$M_L=-1$	$J_e=2$	$M_J=-1$
State 7:	$M_S=-1$	$M_L=1$	$J_e=0$	$M_J=0$
State 8:	$M_S=0$	$M_L=0$	$J_e=1$	$M_J=0$
State 9:	$M_S=1$	$M_L=-1$	$J_e=2$	$M_J=0$
State 10:	$M_S=0$	$M_L=1$	$J_e=1$	$M_J=1$
State 11:	$M_S=1$	$M_L=0$	$J_e=2$	$M_J=1$
State 12:	$M_S=1$	$M_L=1$	$J_e=2$	$M_J=2$

The first three sublevels belong to the ground state, and the other nine sublevels to the excited state. We will use either representation, depending on which one best fits our purposes. States in L, M_L, S, M_S will be denoted by the subscript ''u'' (uncoupled), while states in the J, M_J representation will be denoted by the subscript ''c'' (coupled).

Passing from one representation to the other is accomplished by means of the transformation matrix whose elements are Clebsch-Gordan coefficients. In particular, states 1 through 4 and state 12 are the same in both representations. The other states are linked by the relations

$$\begin{pmatrix} \psi_{5u} \\ \psi_{6u} \end{pmatrix} = A_{-1} \begin{pmatrix} \psi_{5c} \\ \psi_{6c} \end{pmatrix}, \tag{3.1a}$$

$$\begin{pmatrix} \psi_{7u} \\ \psi_{8u} \\ \psi_{9u} \end{pmatrix} = A_0 \begin{pmatrix} \psi_{7c} \\ \psi_{8c} \\ \psi_{9c} \end{pmatrix}, \tag{3.1b}$$

$$\begin{pmatrix} \psi_{10u} \\ \psi_{11u} \end{pmatrix} = A_{+1} \begin{pmatrix} \psi_{10c} \\ \psi_{11c}, \end{pmatrix} \tag{3.1c}$$

where A_{-1}, A_0, and A_{+1} are matrices of transformation that contain the appropriate Clebsch-Gordan coefficients.

Details of the spin-orbit coupling need not be known. The only parameters needed to carry out the calculations are the energy displacements from the unperturbed $L=1$ level introduced by the coupling. The Hamiltonian in the L, M_L, S, M_S representation is not diagonal even in the absence of the electromagnetic field, but its evaluation is straightforward: using the transformation (3.1), we can write

$$\langle m,\mu|H_0|m',\mu'\rangle = \sum_{JM_J} \sum_{J'M'_{J'}} c(m,\mu,J,M_J)c(m',\mu',J',M'_{J'})\langle J,M_J|H_0|J',M'_{J'}\rangle = \sum_{JM_J} c(m,\mu,J,M_J)c(m',\mu',J,M_J)E_J, \tag{3.2}$$

where m,μ, and m',μ' denote the orbital and spin z components of two states in the uncoupled representation, and $c(m,\mu,J,M_J)$, $c(m',\mu',J',M'_{J'})$ are Clebsch-Gordan coefficients. E_J is the energy of the Jth level displaced by the spin-orbit coupling.

The atomic polarization can also be evaluated in either representation. Defining the vectors

$$\boldsymbol{\epsilon}_+ = -\frac{\hat{\boldsymbol{\imath}} + i\hat{\boldsymbol{\jmath}}}{\sqrt{2}}, \tag{3.3a}$$

$$\boldsymbol{\epsilon}_- = \frac{\hat{\boldsymbol{\imath}} - i\hat{\boldsymbol{\jmath}}}{\sqrt{2}} \tag{3.3b}$$

and using Eqs. (2.5) the electric dipole operator **d** is expressed in spherical components

$$\mathbf{d} = T_{+1}\boldsymbol{\epsilon}_+^* + T_{-1}\boldsymbol{\epsilon}_-^* + z\mathbf{k}, \tag{3.4}$$

where the asterisk denotes the complex conjugate. Assuming that the atomic system is in a pure, quantum mechanical state, and expanding the atomic wave function $|\psi\rangle$ in terms of the eigenvectors $|\phi_n\rangle$ of the chosen basis, we find the expectation value of **d**:

$$\langle \mathbf{d} \rangle = \sum_n \sum_{n'} c_{n'}^* c_n \langle \phi_{n'} | T_{+1}\boldsymbol{\epsilon}_+^* + T_{-1}\boldsymbol{\epsilon}_-^* + z\mathbf{k} | \phi_n \rangle. \tag{3.5}$$

In the L, M_L, S, M_S representation, $\langle \mathbf{d} \rangle$ is given by

$$\begin{aligned}\langle \mathbf{d} \rangle = \Re\{&\mathcal{C}(0,+1,+1)(c_{1u}c_{7u}^* + c_{2u}c_{10u}^* + c_{3u}c_{12u}^*)\boldsymbol{\epsilon}_+^* + \mathcal{C}(0,-1,-1)(c_{1u}c_{4u}^* + c_{2u}c_{6u}^* + c_{3u}c_{9u}^*)\boldsymbol{\epsilon}_-^* \\ &+ \mathcal{C}(0,0,0)(c_{1u}c_{5u}^* + c_{2u}c_{8u}^* + c_{3u}c_{11u}^*)\mathbf{k}\} + \text{c.c.},\end{aligned} \tag{3.6}$$

where the coefficients $\mathcal{C}(m,q,m')$ are given by

$$\mathcal{C}(m,q,m') = \frac{\langle J_g, K, m, q | J_g, K, J_e, m' \rangle}{\sqrt{2J_e + 1}} \tag{3.7}$$

with $J_g = L_g = 0$ and $J_e = L_e = 1$, and $\Re$ is the reduced matrix element of the operator **d** for the transition $L = 0 \leftrightarrow L = 1$. Note that the electric dipole operator couples states with the same spin component, since it involves the electron coordinates only.

In the J, M_J representation, there are three distinct transitions, connecting the ground state with each level belonging to the multiplet. The expectation value of the electric dipole operator is given by

$$\begin{aligned}\langle \mathbf{d} \rangle = k\{&-\Re_0\mathcal{C}_0(0,0,0)c_{7c}^*c_{2c} + \Re_1[\mathcal{C}_1(-1,0,-1)c_{5c}^*c_{1c} + \mathcal{C}_1(0,0,0)c_{8c}^*c_{2c} + \mathcal{C}_1(+1,0,+1)c_{10c}^*c_{3c}] \\ &- \Re_2[\mathcal{C}_2(-1,0,-1)c_{6c}^*c_{1c} + \mathcal{C}_2(0,0,0)c_{9c}^*c_{2c} + \mathcal{C}_2(+1,0,+1)c_{11c}^*c_{3c}]\} + \boldsymbol{\epsilon}_+^*\{-\Re_0\mathcal{C}_0(-1,+1,0)c_{7c}^*c_{1c} \\ &+ \Re_1[\mathcal{C}_1(-1,+1,0)c_{8c}^*c_{1c} + \mathcal{C}_1(0,+1,+1)c_{10c}^*c_{2c}] - \Re_2[\mathcal{C}_2(-1,+1,0)c_{9c}^*c_{1c} + \mathcal{C}_2(0,+1,+1)c_{11c}^*c_{2c} \\ &+ \mathcal{C}_2(+1,+1,+2)c_{12c}^*c_{3c}]\} + \boldsymbol{\epsilon}_-^*\{-\Re_0\mathcal{C}_0(+1,-1,0)c_{7c}^*c_{3c} + \Re_1[\mathcal{C}_1(0,-1,-1)c_{5c}^*c_{2c} + \mathcal{C}_1(+1,-1,0)c_{8c}^*c_{3c}] \\ &- \Re_2[\mathcal{C}_2(-1,-1,-2)c_{4c}^*c_{1c} + \mathcal{C}_2(0,-1,-1)c_{6c}^*c_{2c} + \mathcal{C}_2(+1,-1,0)c_{9c}^*c_{3c}]\},\end{aligned} \tag{3.8}$$

where the reduced matrix elements for the three distinct transitions are defined as

$$\Re_0 = (g\|T\|e, J=0), \quad \Re_1 = (g\|T\|e, J=1),$$

$$\Re_2 = (g\|T\|e, J=2), \tag{3.9}$$

and the $\mathcal{C}_k(m,q,m_k')$ coefficients are given by

$$\mathcal{C}_k(m,q,m_k') = \frac{\langle J_g, 1, m, q | J_g, 1, J_k', m_k' \rangle}{\sqrt{2j_k' + 1}} \tag{3.10}$$

The two expressions (3.6) and (3.8) must yield the same result for the expectation value of the dipole electric operator, which is of course independent of the representation. This sets a relationship among the reduced matrix elements in the two equations,

$$\Re_0 = -\frac{\Re}{\sqrt{3}}, \quad \Re_1 = \Re, \quad \Re_2 = -\sqrt{\frac{5}{3}}\,\Re. \tag{3.11}$$

These equations can also be proved directly by using the transformations (3.1) and replacing the Clebsch-Gordan coefficients by their actual values.

If the atomic system is not prepared in a pure, quantum mechanical state, the coefficients c_u or c_c in the expressions (3.6) or (3.8) must be replaced by the density matrix elements,

$$\sigma_{mn} = \langle c_m c_n^* \rangle. \tag{3.12}$$

Let the transformation matrix between the c_u and c_c coefficients be denoted by **Q**:

$$\{c_u\} = \mathbf{Q}\{c_c\}; \tag{3.13}$$

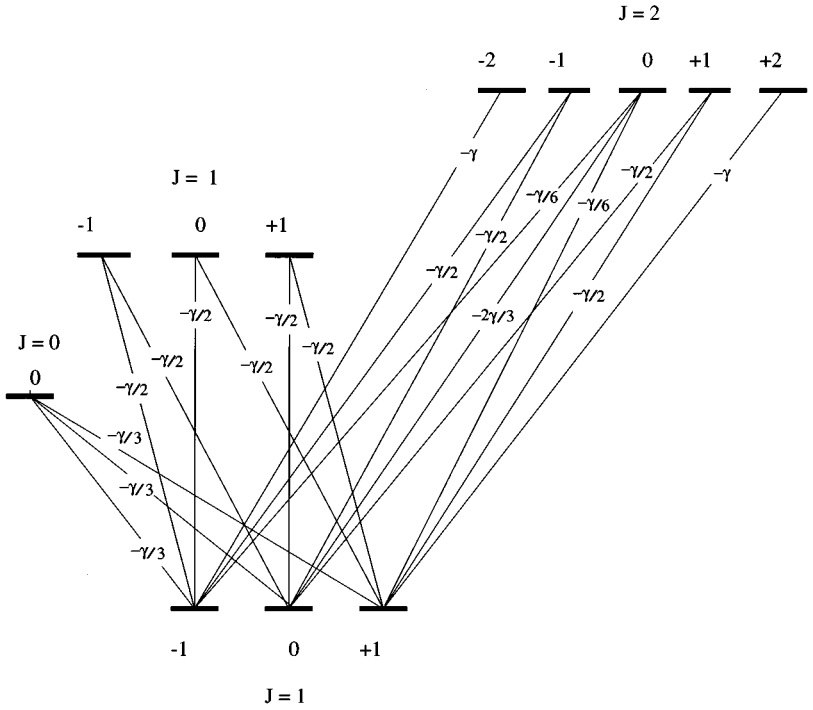

FIG. 2. The energy level diagram for the whole system. The spontaneous emission damping rates are shown for all transitions.

the transformation of the density matrix is then given by

$$\hat{\sigma}_{(LSM_LM_S)} = \mathbf{Q}\hat{\sigma}_{(JM_J)}\mathbf{Q}^{-1}. \tag{3.14}$$

The matrix $\mathbf{Q}$ transforms also the atomic Hamiltonian H_0, not diagonal in the representation L,S,M_L,M_S, into the diagonal form of the J,M_J representation:

$$H_0^{(c)} = \mathbf{Q}^{-1}H_0^{(u)}\mathbf{Q}. \tag{3.15}$$

IV. OPTICAL BLOCH EQUATIONS IN SPIN-ORBIT COUPLING

The Bloch equations for the atomic system under consideration are easily written in the L,M_L,S,M_S representation, and transformed back into the J, M_J representation by applying the transformations (3.14). We will see in this section that, when the frequency separation among the levels in the excited multiplet are much larger than the decay rate γ and the reduced Rabi frequency $\mathcal{E}\mathfrak{R}$, no interference effects arise among the optical transitions, and the transformed equations in the J, M_J representation look the same as those derived in Sec. II.

In the L,M_L,S,M_S representation, the Hamiltonian H_F for the atom-field interaction is very simple. Only those sublevels having the same spin component are coupled by the electric dipole operator. Looking at Table I, we find that the σ_- component of the field couples the states 1-4, 2-6, and 3-9, while the σ_+ component of the field couples the states 1-7, 2-10, 3-12. Thus,

$$\langle 1|H_F|4\rangle = \mathcal{E}'\mathfrak{R}e^{ik_Lz}, \tag{4.1}$$

$$\langle 1|H_F|7\rangle = \mathcal{E}\mathfrak{R}e^{-ik_Lz}, \tag{4.2}$$

and so on. The rotating wave approximation has been adopted here so that the fast oscillating terms have disappeared from the equations. This approximation introduces other, diagonal, terms in the atom-field interaction Hamiltonian, namely,

$$(H_{\mathrm{RWA}})_{kk} = -\delta_L \quad (k=4,5,\ldots,12), \tag{4.3}$$

where δ_L is the frequency detuning of the laser field from the atomic resonance ω_0:

$$\delta_L = \omega_L - \omega_0. \tag{4.4}$$

To these terms we must also add the terms arising from the spin-orbit Hamiltonian $H_0^{(u)}$ derived in the previous section.

The optical Bloch equations in the L,M_L,S,M_S representation are then completed by introducing the damping terms. The raising and lowering operators are easily derived in this representation. The only nonzero terms in the $S_\uparrow$ operator for σ_+ transitions are

$$\langle 7|S_\uparrow^{(+)}|1\rangle = \langle 10|S_\uparrow^{(+)}|2\rangle = \langle 12|S_\uparrow^{(+)}|3\rangle = \sqrt{\gamma}. \tag{4.5}$$

Similarly, we find

$$\langle 5|S_\uparrow^{(0)}|1\rangle = \langle 8|S_\uparrow^{(0)}|2\rangle = \langle 11|S_\uparrow^{(0)}|3\rangle = \sqrt{\gamma}, \tag{4.6}$$

$$\langle 4|S_\uparrow^{(-)}|1\rangle = \langle 6|S_\uparrow^{(-)}|2\rangle = \langle 9|S_\uparrow^{(-)}|3\rangle = \sqrt{\gamma}. \tag{4.7}$$

The matrix elements of the lowering operators $S_\downarrow$ are found by transposing the matrices $S_\uparrow$. Alternatively, the equations can be written in the J,M_J representation. The main assumption here is that the damping constant γ is not affected by the introduction of the spin-orbit coupling, so that it can be taken to be the same for each level in the multiplet.

A quick way of passing from one representation to the other is to use the transformation (3.14), which holds true also for the time derivative of the density operator, since the transformation matrix $\mathbf{Q}$ does not depend explicitly on time.

In Fig. 2 the energy level diagram is shown for the whole system. The allowed transitions are indicated as straight lines connecting the levels, with the decay rate reported for each transition.

These equations, when transformed to the J,M_J representation, reduce to the ones derived in Sec. II, if the frequency separation among the levels in the multiplet is much larger than the reduced Rabi frequency $\Re\mathcal{E}$ and the damping constant γ. In this case, only one level in the multiplet can be excited at a time, depending on which transition the laser field has been tuned to: populations and coherences of those levels that are far off resonance become negligible. For instance, if these conditions are met and the laser field is tuned at the resonance $J_g=1\leftrightarrow J_e=2$, the terms in the Bloch equations arising from Eq. (2.14) are, for the ground sublevels (see also Fig. 2)

$$\left(\frac{\partial\sigma_{11}}{\partial t}\right)_{\text{damp}}=\gamma\,\frac{6\sigma_{44}+3\sigma_{66}+\sigma_{99}}{6}, \tag{4.8a}$$

$$\left(\frac{\partial\sigma_{22}}{\partial t}\right)_{\text{damp}}=\gamma\,\frac{3\sigma_{66}+4\sigma_{99}+3\sigma_{1111}}{6}, \tag{4.8b}$$

$$\left(\frac{\partial\sigma_{33}}{\partial t}\right)_{\text{damp}}=\gamma\,\frac{\sigma_{99}+3\sigma_{1111}+6\sigma_{1212}}{6}, \tag{4.8c}$$

$$\left(\frac{\partial\sigma_{13}}{\partial t}\right)_{\text{damp}}=\gamma\,\frac{\sqrt{6}\sigma_{49}+3\sigma_{611}+\sqrt{6}\sigma_{912}}{6}. \tag{4.8d}$$

These terms are the same as those that would be found from Eq. (2.14) for a single $J_g=1\leftrightarrow J_e=2$ transition.

The construction of the optical Bloch equations in the J,M_J representation from a transformation of the equations in the L,M_L,S,M_S representation has several advantages: in the first instance, the damping terms in the latter representation are far easier to handle, since its Zeeman structure is simpler. Second, one has to deal only with those coherences that arise between sublevels having the same spin component, since the electric dipole interaction with the field does not change the electronic spin or the nuclear quadrupole components. As a matter of fact, the transformation into the J,M_J representation brings in coherences among Zeeman sublevels belonging to *different* levels in the multiplet, a feature that could hardly be inferred when working directly in this representation.

The cooling force can be found, as for the single transition case, by integrating the system of differential equations until a stationary regime is found, and then evaluating the atomic polarization from Eqs. (3.6) or (3.8), depending on which representation has been used. Alternatively again, one can solve the linear system for the stationary case directly, as discussed in Sec. II. The transformation (2.15), (2.16) still applies, with each diagonal τ_{kk} element in Eq. (2.16) written in the form $\exp(im_k\phi)$ where m_k is the magnetic quantum number of the kth state (see Table I).

V. THE COOLING FORCE IN STRONG SPIN-ORBIT COUPLING

We pass now to the discussion of the cooling force exerted by the two counterpropagating waves of opposite circular polarizations onto the atom in the atomic level configuration described in the previous sections. First we consider the case where the spin-orbit coupling is strong enough that the frequency separation among the levels in the excited multiplet is larger than the reduced Rabi frequency and the decay rate γ of the excited states. We set the values of the coupling parameters so that the frequency separations are 50γ between the $J=0$ and $J=1$ excited levels, and 71γ between the $J=1$ and $J=2$ excited levels in the multiplet. The transition frequencies will be denoted by ω_0 (ground state to $J=0$ excited state), ω_1 (ground state to $J=1$ excited state), and ω_2 (ground state to $J=2$ excited state).

In what follows, the frequencies will be expressed in units of γ, while the atomic velocities will be expressed in units of γ/k_L, where k_L is the wave vector of the laser fields. Since there are several optical transitions in the atomic system, each one having its own strength (or electric dipole), the definition of the Rabi frequency needs some clarification. We have preferred to introduce a ''reduced Rabi frequency'' (RRF, see Sec. II, which involves the reduced matrix elements of the bare transition $L=0\leftrightarrow L=1$. In terms of that RRF, all the electric-dipole matrix elements, specific to our system, can be evaluated (see Sec. III). In other words, the Rabi frequency is defined as the largest one among the various Rabi frequencies associated to the different transitions, typically the one connecting the $|m|=J_g$ sublevels of the ground state to the $|m|=J_e$ sublevels of the excited state, which have the largest Clebsch-Gordan coefficients. In Sec. III one can find the reduced matrix elements $\Re_0$, $\Re_1$, and $\Re_2$ of the transitions between the ground state and the excited multiplet, expressed as a function of $\Re$, the reduced matrix elements for the transition $L=0\leftrightarrow L=1$, and deduce from them the corresponding Rabi frequencies for the various transitions. The RRF is therefore defined as $\mathcal{E}\Re/\hbar$, where $\mathcal{E}$ is the amplitude of the laser field; see Eqs. (2.3).

In several situations, it is expedient to introduce a new quantization axis, lying on the plane x-y and directed along the electric field component, as experienced by the atom, that results from the superposition of the σ_+ and σ_- polarized fields. The direction of the new quantization axis depends on the z coordinate, and if the atom is moving along the z axis, it varies with time. The transformation of the state amplitudes of the ground state under such change of the quantization axis is accomplished by the unitary transformation

$$\tau'=\begin{pmatrix}\dfrac{e^{i\phi}}{2} & -\dfrac{1}{\sqrt{2}} & \dfrac{e^{-i\phi}}{2}\\[2ex] \dfrac{e^{i\phi}}{\sqrt{2}} & 0 & -\dfrac{e^{-i\phi}}{\sqrt{2}}\\[2ex] \dfrac{e^{i\phi}}{2} & \dfrac{1}{\sqrt{2}} & \dfrac{e^{-i\phi}}{2}\end{pmatrix} \tag{5.1}$$

where $\phi=k_L v t$. Similar transformations apply for the state

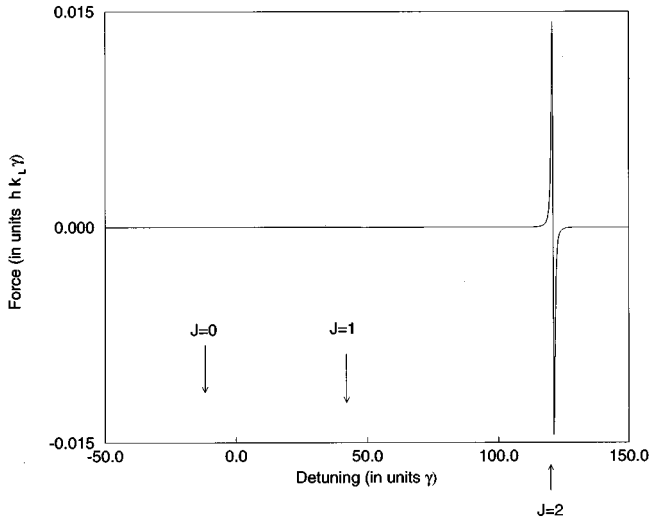

FIG. 3. Force (units $\hbar k_L \gamma$) vs laser detuning (units γ).

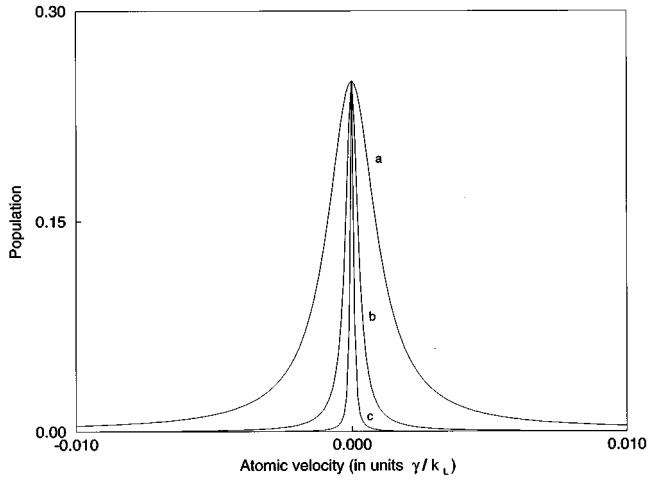

FIG. 5. Ground-state populations vs atomic velocity in the stationary regime. The laser field is tuned at the ω_0 resonance.

amplitudes of the excited states. The new reference frame will be referred to as the ''primed'' system.

In Fig. 3 we show the cooling force plotted versus the detuning δ_L of the laser field defined with respect to the transition occurring between the ground state and the $J=0$ excited state, $\delta_L=\omega_L-\omega_0$. The atomic velocity is kept fixed at $v=-0.1\gamma/k_L$. The laser frequency spans the entire interval containing the frequencies of the excited multiplet, but an appreciable cooling force appears only about the transition involving the $J=2$ excited state. The force is positive (i.e., opposite to the direction of the atomic motion) when the field is tuned just below the atomic transition, and negative on the other side.

In Fig. 4 we show the same graph as in Fig. 3, expanded about the only resonance ($J_g=1\leftrightarrow J_e=2$) that displays an appreciable cooling force. In this graph are shown the plots for an atomic velocity $v=-0.1\gamma/k_L$ (solid curve) and $v=-0.002\gamma/k_L$ (dashed curve). The cooling force as a function of the atomic velocity, for a fixed laser frequency tuned at 0.5γ below the ω_2 transition, reproduces the graph shown in Fig. 1(a) ($J_g=1\leftrightarrow J_e=2$ transition), as expected because of the large frequency differences in the excited multiplet.

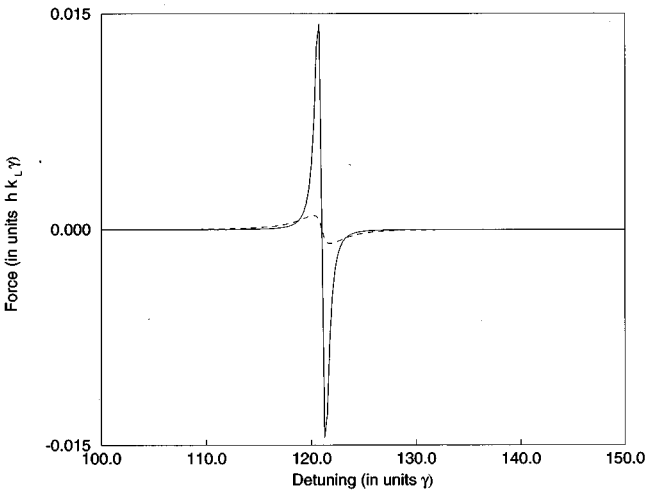

FIG. 4. Force (units $\hbar k_L \gamma$) vs laser detuning (units γ).

When the frequency separations among the levels in the excited multiplet are sufficiently large, the two transitions at ω_0 and ω_1 are not usable to cool the atomic system. We give here a brief explanation of the absence of *any* laser cooling (i.e., both Doppler and sub-Doppler) for these transitions, which generalizes to the high intensity regime the results of Ref. [8].

When the laser frequency is tuned close to the ω_0 transition, and the two other transitions at ω_1 and ω_2 are far off resonance, there is no appreciable transfer of population in the upper $J_e=0$ level of the excited multiplet for the present polarization configuration; in the ground state, population accumulates in the $m=0$ Zeeman sublevel (quantization axis parallel to the propagation vector of the electromagnetic field, unprimed frame), except for a tiny interval of atomic velocities around $v=0$. In Fig. 5 we show the population of the Zeeman sublevel $m=-1$ of the ground state in the stationary regime, versus the atomic velocity v, for several frequency separations in the excited multiplet. The Zeeman sublevel $m=1$ gets the same population as the $m=-1$ sublevel. The laser frequency is tuned at the ω_0 resonance, but the graph would be similar also for small detunings from that resonance. When $|\omega_2-\omega_0|$ and $|\omega_1-\omega_0|$ are very large when compared to γ, the velocity interval over which the Zeeman sublevels $m=\pm 1$ get an appreciable stationary population shrinks [see Figs. 5(a)–5(b)]. At infinite frequency separation [see Fig. 5(c)], the atomic system may end up in a variety of stationary regimes, i.e., the Zeeman sublevel $m=0$ of the ground state may get any population in the stationary regime at $v=0$, the remaining population being equally shared among the two other ground sublevels, while for $v\neq 0$, the entire population remains in the $m=0$ sublevel, leaving the other two sublevels of the ground state empty.

This is easily understood if we change the quantization axis of the atomic system to the primed frame. Let us assume that we have prepared the system in an incoherent superposition of ground state sublevels, referring to the quantization axis along the z axis, and let σ_{11}, σ_{33} be the initial populations of the $m=-1$ and $m=1$ Zeeman sublevels. The atom is assumed to be at rest in the laboratory frame. We then rotate the quantization axis and pass to the primed reference

frame. In the new quantization configuration, the electric field appears to be linearly polarized, so that there is just one optical transition connecting the $m=0$ Zeeman sublevel of the ground state to the (unique) $m=0$ excited sublevel. Also, a coherence σ_{13} arises among the $m=-1$ and $m=1$ Zeeman sublevels of the ground state, equal to $3(\sigma_{11}+\sigma_{33})/4-1/2$. The subsequent interaction with the field does not involve these Zeeman sublevels, so that, in the transient time during which the stationary regime is reached, the coherence σ_{13} remains unchanged. The field acts on the system by pumping population up from the ground $m=0$ sublevel to the excited state, from which it decays to all three ground sublevels. In the primed frame, the Zeeman $m=\pm 1$ sublevels act as a sink for the population, which cannot escape from them. Hence, when the stationary regime is reached, we find that the population is shared between these sublevels, while the $m=0$ sublevel is empty. This is the final density matrix of the atomic system for the primed quantization axis. Transforming back to the original quantization axis, we find the density matrix of the ground sublevels of the form

$$\sigma=\begin{pmatrix} \frac{3(\sigma_{11}+\sigma_{33})}{8} & 0 & \frac{3(\sigma_{11}+\sigma_{33})}{8} \\ 0 & 1-\frac{3(\sigma_{11}+\sigma_{33})}{4} & 0 \\ \frac{3(\sigma_{11}+\sigma_{33})}{8} & 0 & \frac{3(\sigma_{11}+\sigma_{33})}{8} \end{pmatrix}. \tag{5.2}$$

Since σ_{11} and σ_{33} are arbitrary, the final state for such a transition is dependent on the initial preparation, and may have any population in the range 0 through 3/8 in each of the sublevels with $m=\pm 1$, with the remaining population in the $m=0$ sublevel of the ground state. Thus, different population distribution can be found in the final state. It is precisely the coherence between the $m=-1$ and $m=1$ ground sublevels (in the unprimed quantization configuration) that prevents the population from being pumped out of these sublevels, by the two circularly polarized fields, into the $m=0$ sublevel. In an incoherent transition, population would pass continuously from the $m=-1$, $m=1$ sublevels into the $m=0$ sublevel (through photon absorption processes followed by spontaneous emission processes), until the former are completely emptied.

The presence of different stationary states for the $J_g=1\leftrightarrow J_e=0$ transition at $v=0$ is confirmed by evaluating the eigenvalues of the time evolution matrix for the matrix elements of the density operator. One of these eigenvalues is always zero, corresponding to the existence of a constant of motion (the sum of the levels' population). At $v=0$, however, two eigenvalues have the common value of zero, as shown in Fig. 6, while all other eigenvalues have their real part negative, as expected. At $v=0$ there are two constants of motion: however we prepare the system at the initial time, we find that the final population of each of the two sublevels of the ground state, (the $m=-1$ and $m=+1$ sublevels) gets a steady state population equal to $3(\sigma_{11}+\sigma_{33})/8$.

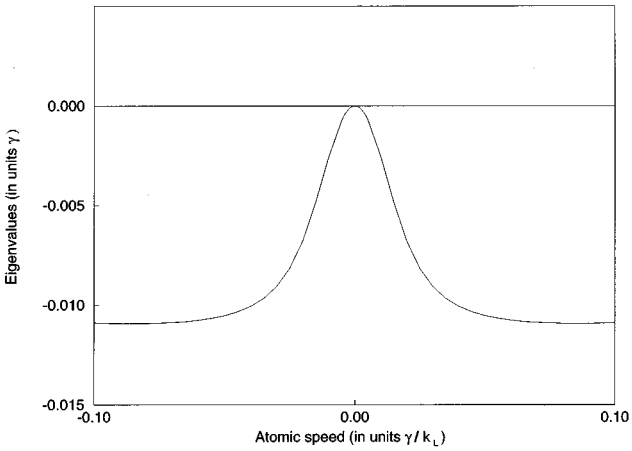

FIG. 6. Two eigenvalues of the evolution matrix merge at 0 when the atom speed v is null. One eigenvalue is zero for any v. The eigenvalues are in units of γ. A null eigenvalue corresponds to a constant of motion.

This is a very unstable situation, though, since any small perturbation of the σ_{13} coherence would disrupt the interference process between the two transitions, leading to a small, but efficient, channel of complete population depletion of the $m=\pm 1$ sublevels. This occurs as soon as the atom gets a thermal speed by fluctuations or a kick by collisions with its environment. It should be noted, however, that in the case of finite frequency separations in the excited manifold, as the one depicted in Fig. 5, such instability is eliminated by the very presence of the other excited levels: these remove the degeneracy of the two eigenvalues that are zero at $v=0$. In any case, there is no magnetic alignment in the ground state, nor any appreciable transfer of population in the upper ($J_e=0$) state, hence no atomic polarization. Thus, no cooling force can arise when the laser field is tuned near the ω_0 resonance.

Similar considerations apply for the isolated $J_g=1\leftrightarrow J_e=1$ transition, although the atomic system reaches in this case a stationary regime that is unique for any atomic speed, and independent of the initial conditions (no degeneracy is found in the eigenvalues of the time evolution matrix of the density operator elements). Rotating the quantization axis to the primed frame, the resulting linearly polarized field induces transitions between sublevels having the same magnetic quantum number (referring to the new quantization axis), except the $m_g=0\leftrightarrow m_e=0$ transition, forbidden by the selection rules. At $v=0$, the system ends up in a stationary regime in which the $m_g=0$ sublevel is fully populated, while all other elements in the density matrix are zero. Transforming back to the original configuration of the quantization axis (along the z axis), we find that the populations of the $m_g=-1$ and $m_g=+1$ Zeeman sublevels are equally populated to 1/2 and the $m_g=0$ sublevel is empty. Again, coherence between the $m_g=-1$ and $m_g=+1$ Zeeman sublevels prevents population transfer into the excited sublevel $m_e=0$, so that the excited state remains completely unpopulated, and no fluorescence can be detected from atoms at rest.

This symmetry is broken when the atom moves along the z axis. In the primed frame, the Hamiltonian of the system is written as

$$H_0' = \begin{pmatrix} 0 & -\frac{k_L v}{\sqrt{2}} & 0 & -\sqrt{2}\mathcal{E} & 0 & 0 \\ -\frac{k_L v}{\sqrt{2}} & 0 & -\frac{k_L v}{\sqrt{2}} & 0 & 0 & 0 \\ 0 & -\frac{k_L v}{\sqrt{2}} & 0 & 0 & 0 & \sqrt{2}\mathcal{E} \\ -\sqrt{2}\mathcal{E} & 0 & 0 & -\delta_L & -\frac{k_L v}{\sqrt{2}} & 0 \\ 0 & 0 & 0 & -\frac{k_L v}{\sqrt{2}} & -\delta_L & -\frac{k_L v}{\sqrt{2}} \\ 0 & 0 & \sqrt{2}\mathcal{E} & 0 & -\frac{k_L v}{\sqrt{2}} & -\delta_L \end{pmatrix} \tag{5.3}$$

[sublevels are labeled as in Eq. (2.16)]. Equation (5.3) shows that in the primed frame, a motional coupling arises that couples $m=-1$ to $m=0$ and $m=0$ to $m=+1$ within each manifold, see Ref. [6]. This Hamiltonian is time independent and can be diagonalized numerically. The equation of motion for the density operator can be easily integrated, and one finds the final (stationary) density matrix to be of the form

$$\sigma' = \begin{pmatrix} a & \alpha^* & a & c & 0 & -c \\ \alpha & b & \alpha & \beta & 0 & -\beta \\ a & \alpha^* & a & c & 0 & -c \\ c & \beta^* & c & d & 0 & -d \\ 0 & 0 & 0 & 0 & 0 & 0 \\ -c & \beta^* & -c & -d & 0 & d \end{pmatrix} \tag{5.4}$$

as could be expected from Eq. (5.3), on the grounds of symmetry considerations. In Eq. (5.4), latin letters denote real, positive quantities and greek letters complex quantities. Transforming back to the original quantization frame, we see that the $m_g=+1$ and $m_g=-1$ sublevels get highly unbalanced populations,

$$\sigma_{-1,-1} = a + \frac{b}{2} + \frac{\alpha}{\sqrt{2}} + \frac{\alpha^*}{\sqrt{2}}, \tag{5.5a}$$

$$\sigma_{+1,+1} = a + \frac{b}{2} - \frac{\alpha}{\sqrt{2}} - \frac{\alpha^*}{\sqrt{2}}, \tag{5.5b}$$

while the $m_g=0$ remains empty. Contrary to the $v=0$ situation, however, there is population in the excited, $m_e=0$ sublevel, and hence fluorescence can be detected from moving atoms. This phenomenon, according to which fluorescence disappears when the atoms approaches a condition of zero kinetic energy, is known as ''coherent population trapping'' [14]. It can also lead to very cold atomic distributions (see Ref. [15] for a recent review of the subject).

In spite of the large, unbalanced population distribution between the Zeeman sublevels with $m_g=\pm 1$, no radiative force is exerted onto the atom. This can be seen, for instance, by looking at the optical coherences of the stationary density operator in the unprimed frame. These turn out to be equal to

$$\sigma_{-1_g,0_e} = -\beta - \sqrt{2}c, \tag{5.6a}$$

$$\sigma_{1_g,0_e} = \beta - \sqrt{2}c; \tag{5.6b}$$

their imaginary parts, which stem from β, are opposite in sign. Taking into account Eq. (2.18), and recalling that $\mathcal{C}(m,+1,\alpha)$ and $\mathcal{C}(m,-1,\alpha)$ are also opposite in sign for the $J_g=1 \leftrightarrow J_e=1$ transition, the radiative force (2.20) is null. In Ref. [8] it is shown that the reactive and dissipative components of the force for this transition, in the weak field limit, are equal in size and opposite in sign, so that they mutually cancel.

Thus, in our model, the only radiative force may arise from the $J_g=1 \leftrightarrow J_e=2$ transition, which will be referred to as the main transition. A brief description of the origin of the force has been given in Sec. II. A deeper analysis can be found in Refs. [6,8]. In spite of the fact that the two transitions $J_g=1 \leftrightarrow J_e=0$ and $J_g=1 \leftrightarrow J_e=1$ do not provide any additional force, their effect may be large enough when their frequency separations from the other transition is of the same order of magnitude as the damping constant γ or the reduced Rabi frequency. This will occur when the spin-orbit (SO) coupling is not sufficiently strong to eliminate the interference effects among the various transitions. Removal of the eigenvalue degeneracy in the $J_g=1 \leftrightarrow J_e=0$ transition, due to the presence of other transitions, has been illustrated in this section. Graphs of the radiative force in the weak SO coupling case are presented in the next section.

VI. WEAK SPIN-ORBIT COUPLING

The radiative force is substantially changed when the atomic transition used to cool the atom is close in frequency to other transitions, normally belonging to the same multip-

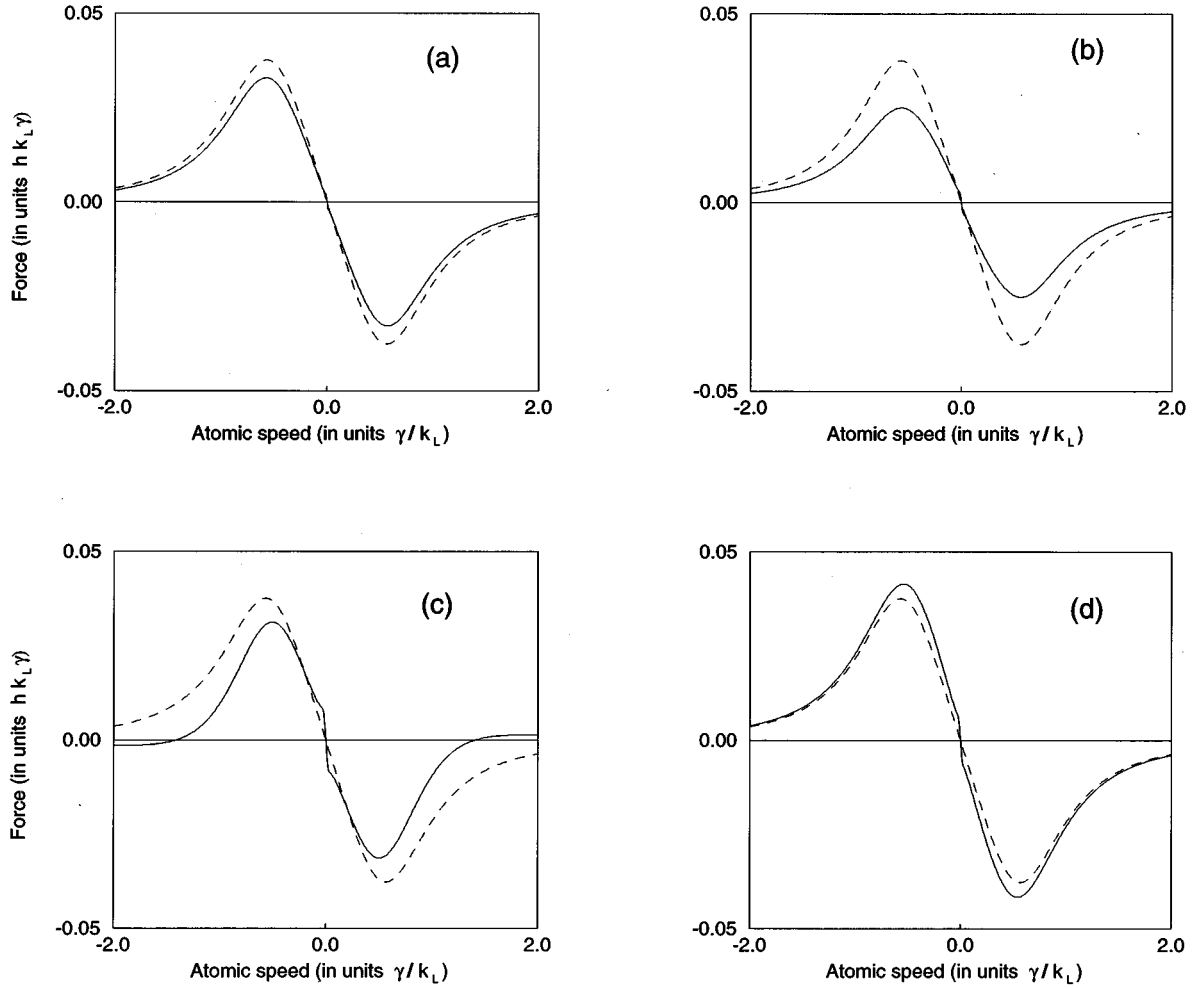

FIG. 7. Cooling force vs atomic speed in the low intensity limit. Spin-orbit coupling increases from graph (a) to graph (d) (solid line). For comparison, in each graph the plot for the $J=0\leftrightarrow J=1$ transition (dashed line) is also shown.

let. We show in this section these modifications, at low (Fig. 7) and high (Fig. 10) field intensities. In this section the value of the reduced Rabi frequency for the low field intensity is set at 0.2795γ while the value for the high field intensity is set at 1.8γ. In all graphs in this section, the laser frequency detuning refers to the $J=1\leftrightarrow J=2$ transition (solid curve). The other two transitions, ($J=1\leftrightarrow J=1$ and $J=1\leftrightarrow J=0$) lie below the first one, and are separated from it by $\delta\omega_{12}=\omega_1-\omega_2$ and $\delta\omega_{02}=\omega_0-\omega_2$, respectively. Hence $\delta\omega_{12}$ and $\delta\omega_{02}$ take only negative values.

In Fig. 7 the radiative force (solid curve) is shown at various spin-orbit coupling values, along with the force pertaining to the $J=0\leftrightarrow J=1$ transition, i.e., the force at zero coupling (dashed curve). The field amplitude is such that the reduced Rabi frequency is 0.28γ, and the laser detuning from the $J=1\leftrightarrow J=2$ transition is $\delta_L=-0.5\gamma$. From Figs. 7(a)–7(d), the spin-orbit coupling increases. In Fig. 7(a), the laser frequency is tuned to the red side of all three transitions ($\delta\omega_{12}=-0.15\gamma$ and $\delta\omega_{02}=-0.4\gamma$). The main effect here is a slight reduction of the Doppler force at its largest value, attained at $v=\pm 0.5\gamma/k_L$. Also, a tiny sub-Doppler force arises at very small atomic speed. This is too small to appear in Fig. 7(a).

In Fig. 7(b), the laser frequency is tuned to the red side of the $J=1\leftrightarrow J=2$ and $J=1\leftrightarrow J=1$ transitions, but to the blue side of the $J=1\leftrightarrow J=0$ transition ($\delta\omega_{12}=-0.3\gamma$ and $\delta\omega_{02}=-0.8\gamma$). A further decrease appears in the Doppler force at its largest value, while the force is slightly modified by magnetic alignment about $v=0$. In Fig. 7(c), the laser frequency is tuned to the blue side of the $J=1\leftrightarrow J=0$ and $J=1\leftrightarrow J=1$ transitions, but these are still close to the $J=1\leftrightarrow J=2$ transition and affect substantially the cooling force ($\delta\omega_{12}=-3\gamma$ and $\delta\omega_{02}=-8\gamma$). A new phenomenon arises in this case: the cooling force changes sign when the atomic speed is larger than γ/k_L, thus limiting the effective range of velocities that can be captured by the radiative force. This is arguably due to the fact that the force here is contributed to by dissipative effects, and by reactive effects. The latter changes its sign, and becomes predominant at large atomic velocities. Application of a bichromatic laser fields of suitable frequencies has been shown to remove these undesirable effects in several atomic level configurations [16,17]. In Fig. 7(d), the spin-orbit coupling is strong enough to eliminate any interference effects among the transitions ($\delta\omega_{12}=-15\gamma$ and $\delta\omega_{02}=-40\gamma$), and the cooling force takes the shape that belongs to an isolated transition. In all cases, the force is symmetric about $v=0$.

Figure 8 shows the radiative force in a short interval of atomic velocities, for a number of values of the coupling strength, starting from the degenerate case of zero coupling,

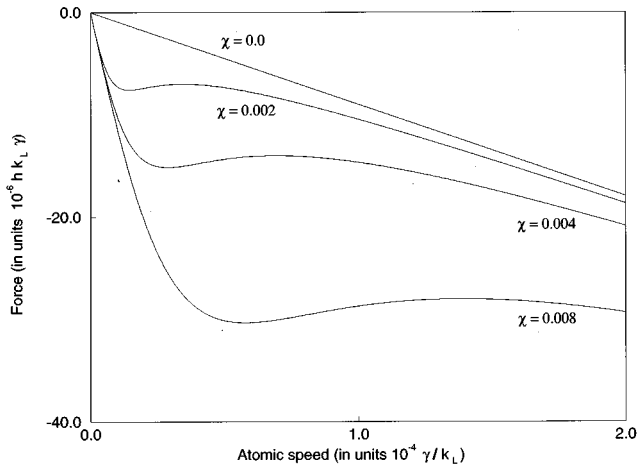

FIG. 8. A sub-Doppler force near $v=0$ appears as soon as level degeneracy is removed. The level splittings are assumed to be proportional to an effective coupling strength. At $\chi=1$ they are $\delta\omega_{02}=-8\gamma$, $\delta\omega_{12}=-3\gamma$. The values of χ shown here are $\chi=0$, $\chi=2\times10^{-3}$, $\chi=4\times10^{-3}$, $\chi=8\times10^{-3}$.

for which no sub-Doppler force exists.

In Fig. 9, we show the friction coefficient α, defined as the derivative of the radiative force with respect to the atomic speed at $v=0$, $F\sim-\alpha v$ if v is sufficiently small. The friction coefficient is plotted versus the strength of the spin-orbit coupling, at low field intensity. The frequency splittings in the multiplet are assumed to be proportional to an effective coupling strength χ, and take the values $\delta\omega_{12}=-3\gamma$ and $\delta\omega_{02}=-8\gamma$ when $\chi=1$. The friction coefficient has a discontinuity as soon as the level degeneracy is removed by the spin-orbit coupling (see Fig. 8), then decreases toward a minimum reached at $\chi=0.18$, and finally tends to the limit value pertaining to the isolated transition $J=1\leftrightarrow J=2$. Although the friction coefficient is very large at small values of χ, the sub-Doppler force affects only a tiny fraction of atoms having very small velocities (see Fig. 8). At $\chi=0.18$, no significant sub-Doppler force exists.

In Fig. 10 we report the graphs (solid curve) for the same

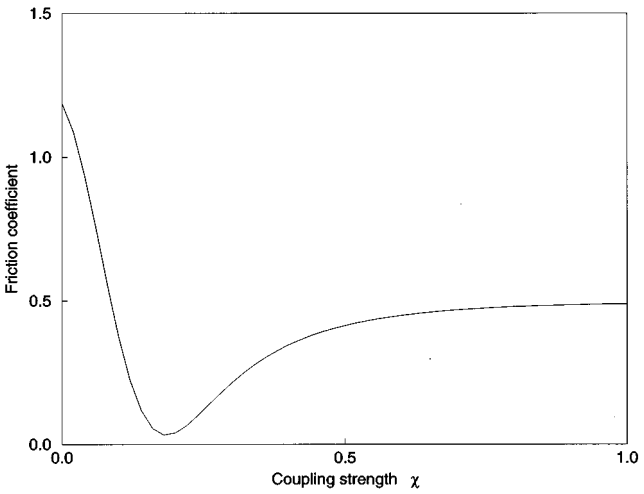

FIG. 9. The friction coefficient vs the coupling strength, low field intensity.

values of the coupling strength as in Fig. 7, but in the strong field regime (reduced Rabi frequency$=1.8\gamma$). The radiative force (dashed curve) at zero coupling is shown again in each graph for comparison. Its shape is consistent with the analytical solution for the $J=0\leftrightarrow J=1$ transition reported in Ref. [18]. The resonances that appear in these graphs when $\chi\neq0$ are due to multiphoton processes: (i) the atom can absorb one photon from the field with circular polarization σ_+, (ii) emit by stimulated emission a photon into the field with circular polarization σ_-, and (iii) absorb another photon from the σ_+ field. Such processes are resonant if the accumulated Doppler shift ($3k_Lv$ in this case) compensates the frequency detuning of the laser field from the main transition (''doppleron'' or velocity-tuned resonances, see Ref. [19]). Note that such a process can occur only if there is magnetic degeneracy in the ground state. Otherwise, after the absorption of a σ_+ photon, there is no transition available for the stimulated emission of a σ_- photon. For this reason, such resonances can appear only for $\chi\neq0$.

The reduction of the velocity capture range is strongly enhanced in the strong field regime [Fig. 10(c), $\chi=1$] The value of χ at which the radiative force takes the form that pertains to the isolated transition $J=1\leftrightarrow J=2$ is much larger than in the weak field regime, and in Fig. 10(d), where $\chi=5$, we still see that the force changes its sign and becomes an antidamping force at large v's. To reach the limiting condition of an isolated transition, the coupling strength must be as large as 50, which corresponds to frequency separation of 150γ and 400γ for $\delta\omega_{12}$ and $\delta\omega_{02}$, respectively, at high field intensity. The friction coefficient about $v=0$, however, is large in the same range of coupling strength (see Fig. 11). In Fig. 12 we show the radiative force for the coupling strength $\chi=50$ (full line), large enough to make the interference effects of the other two transitions negligible [see also Fig. 10(d)]. For comparison (dashed line) the radiative force for $\chi=5$ is also shown.

Finally, we show in Fig. 13 the separate effects of the transitions $J=1\leftrightarrow J=0$ and $J=1\leftrightarrow J=1$ on the radiative force from the main transition $J=1\leftrightarrow J=2$, at high field intensity. In Fig. 13 (solid line), $\delta\omega_{12}$ is very large, so that the only effect on the radiative force comes from the $J=1\leftrightarrow J=0$ transition ($\delta\omega_{02}=-8\gamma$). In Fig. 13 (dashed line) the situation is reversed, with $\delta\omega_{12}=-8\gamma$ and $\delta\omega_{02}=\infty$. The two graphs in Fig. 13 show that the strongest interference effects arise from the $J=1\leftrightarrow J=1$ transition.

VII. CONCLUSIONS

Although the model laser cooling in an atomic system with fine structure interaction presented in this paper is a simplified one (for instance, the ground state is a single $J=1$ state), it shows several features that modify substantially the radiative force as obtained from a ''single transition'' description. Of the three transitions considered in our model, two (namely, the $J=1\leftrightarrow J=0$ and $J=1\leftrightarrow J=1$ transitions) are not capable of yielding any mechanical effects on the atomic motion for this configuration of the electromagnetic fields. Yet, their interference with the main $J=1\leftrightarrow J=2$ transition produces sizable effects when the separation frequency in the excited multiplet is comparable with the damping constant γ of the atomic upper levels. Such

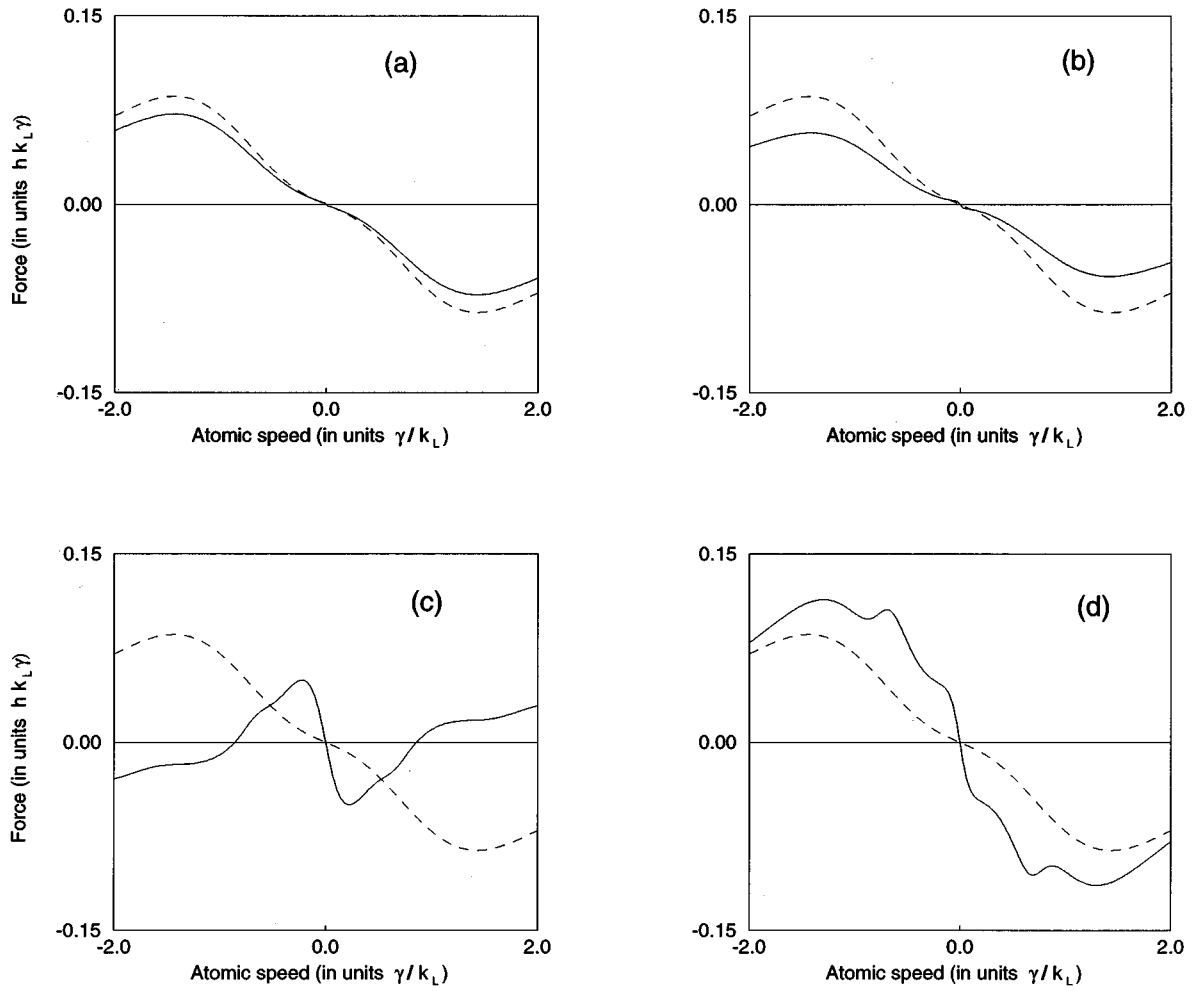

FIG. 10. As in Fig. 7, but in strong field intensity regime.

effects include elimination of any sub-Doppler structure and a redefinition of the velocity capture range.

In real atoms, usually spin-orbit coupling introduces much larger separations in the multiplet structure, and the small separations considered here are more likely to occur in the hyperfine structure of the atomic levels. However, this model can be extended to include effects such as the hyperfine interaction. The coupling of the different angular momenta, orbital, spin, and nuclear, will then be carried out in a suitable order according to the coupling strengths. In such way,

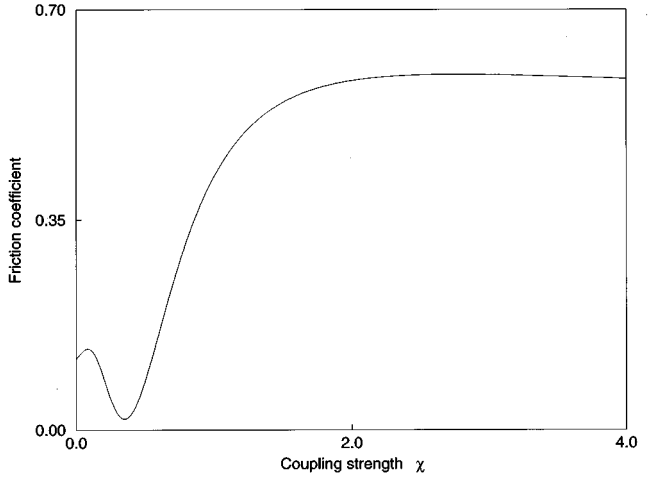

FIG. 11. The friction coefficient (in units $\hbar k_L^2 \gamma$) vs the coupling strength, high field intensity.

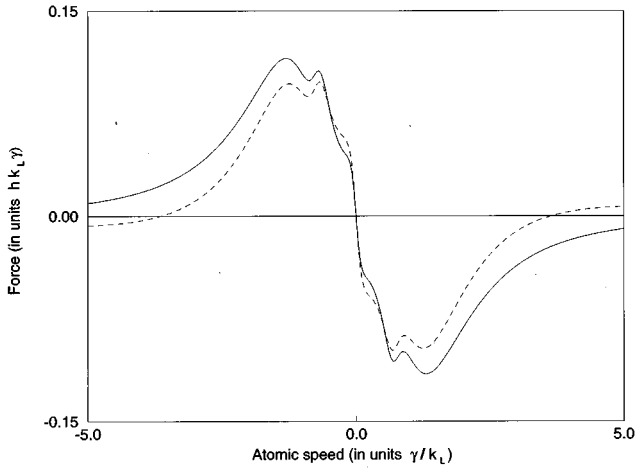

FIG. 12. The radiative force (in units $\hbar k_L \gamma$) vs v, with $\chi = 50$ (solid line) and $\chi = 5$ (dashed line).

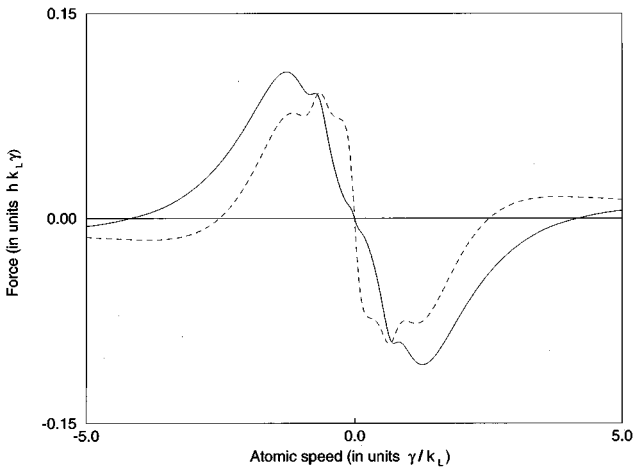

FIG. 13. Effects of the $J=1\leftrightarrow J=0$ (solid line) and $J=1\leftrightarrow J=1$ (dashed line) transitions on the cooling force in the $J=1\leftrightarrow J=2$ transition.

calculations can be done to evaluate the radiative force for real atoms.

Analytical results for the radiative force could in principle be obtained for the low-field-intensity case, but we have preferred not to pursue this goal, in view of the fact that most experiments on atoms having multiplet structure are carried out by using strong fields, usually detuned to the red side of the lowest transition frequency. For such field amplitudes, a fully analytical treatment would probably be impossible. We have limited our discussion to a few examples where the rotation of the quantization axis can be exploited to derive simple results for the density operator that support our conclusions.

ACKNOWLEDGMENT

We wish to thank Professor E. Arimondo for helpful discussions and suggestions during the preparation of the article.

[1] D. Wineland and H. Dehmelt, Bull. Am. Phys. Soc. **20**, 637 (1975).
[2] P. Lett, R. Watts, C. Westbrook, W. D. Phillips, P. Gould, and H. Metcalf, Phys. Rev. Lett. **61**, 169 (1988).
[3] Y. Shevy, D. S. Weiss, P. J. Ungar, and S. Chu, Phys. Rev. Lett. **62**, 1118 (1989).
[4] J. Dalibard, C. Salomon, A. Aspect, E. Arimondo, R. Kaiser, N. Vansteenkiste, and C. Cohen-Tannoudji, in *Proceedings of the 11th Conference on Atomic Physics*, edited by S. Haroche, J. C. Gay, and G. Grynberg (World Scientific, Singapore, 1989).
[5] S. Chu, D. S. Weiss, Y. Shevy, and P. J. Ungar, in *Proceedings of the 11th Conference on Atomic Physics* (Ref. [4]).
[6] J. Dalibard and C. Cohen-Tannoudji, J. Opt. Soc. Am. B **5**, 2023 (1989).
[7] P. J. Ungar, D. S. Weiss, E. Riis, and S. Chu, J. Opt. Soc. Am. B **5**, 2058 (1989).
[8] C. Cohen-Tannoudji, in *Fundamental Systems in Quantum Optics*, Les Houches Summer Session No. LIII, edited by J. Dalibard, J. M. Raimond, and J. Zinn-Justin (Elsevier Science Publishers B.V., Amsterdam, 1991).
[9] Y. Castin and K. Molmer, J. Phys. B **23**, 4101 (1990).
[10] S. Stenholm, Rev. Mod. Phys. **58**, 699 (1986).
[11] C. Cohen-Tannoudji, in *Frontiers in Laser Spectroscopy*, Les Houches Summer Session No. XXVII, edited by R. Balian, S. Haroche, and S. Liberman (North-Holland, Amsterdam, 1977).
[12] M. Ducloy, Phys. Rev. A **8**, 1844 (1973).
[13] A. Omont, Prog. Quantum Electron. **5**, 69 (1977).
[14] G. Alzetta, A. Gozzini, L. Moi, and G. Orriols, Nuovo Cimento B **36**, 5 (1976).
[15] E. Arimondo, in *Progress in Optics*, edited by E. Wolf (Elsevier Science Publisher B.V., Amsterdam, 1996), Vol. XXXV.
[16] A. P. Kazantsev and I. V. Krasnov, J. Opt. Soc. Am. B **6**, 2140 (1989).
[17] T. T. Grove, B. C. Duncan, V. Sanchez-Villicana, and P. L. Gould, Phys. Rev. A **51**, R4325 (1995).
[18] J. Dalibard, S. Reynaud, and C. Cohen-Tannoudji, J. Phys. B **17**, 4577 (1984).
[19] O. Kyrola and S. Stenholm, Opt. Commun. **22**, 123 (1977).